Inter-Beat Interval Estimation with Tiramisu Model: A Novel Approach with Reduced Error

ASIFUL AREFEEN, Arizona State University, USA
ALI AKBARI, Texas A&M University, USA
SEYED IMAN MIRZADEH, Washington State University, USA
ROOZBEH JAFARI, Texas A&M University, USA
BEHROOZ A. SHIRAZI, Washington State University, USA
HASSAN GHASEMZADEH, Arizona State University, USA

Inter-beat interval (IBI) measurement enables estimation of heart-tare variability (HRV) which, in turns, can provide early indication of potential cardiovascular diseases (CVDs). However, extracting IBIs from noisy signals is challenging since the morphology of the signal gets distorted in the presence of noise. Electrocardiogram (ECG) of a person in heavy motion is highly corrupted with noise, known as motion-artifact, and IBI extracted from it is inaccurate. As a part of remote health monitoring and wearable system development, denoising ECG signals and estimating IBIs correctly from them have become an emerging topic among signal-processing researchers. Apart from conventional methods, deep-learning techniques have been successfully used in signal denoising recently, and diagnosis process has become easier, leading to accuracy levels that were previously unachievable. We propose a deep-learning approach leveraging tiramisu autoencoder model to suppress motion-artifact noise and make the R-peaks of the ECG signal prominent even in the presence of high-intensity motion. After denoising, IBIs are estimated more accurately expediting diagnosis tasks. Results illustrate that our method enables IBI estimation from noisy ECG signals with SNR up to -30dB with average root mean square error (RMSE) of 13 milliseconds for estimated IBIs. At this noise level, our error percentage remains below 8% and outperforms other state of the art techniques.

CCS Concepts: • **Applied computing → Life and medical sciences**; *Health informatics*; Consumer health.

Additional Key Words and Phrases: Autoencoder, denoising, electrode motion, inter-beat interval, motion artifacts, tiramisu model

ACM Reference Format:
Asiful Arefeen, Ali Akbari, Seyed Iman Mirzadeh, Roozbeh Jafari, Behrooz A. Shirazi, and Hassan Ghasemzadeh. 2021. Inter-Beat Interval Estimation with Tiramisu Model: A Novel Approach with Reduced Error. *ACM Trans. Comput. Healthcare* 37, 4, Article 111 (July 2021), 20 pages. https://doi.org/10.1145/1122445.1122456

Authors' addresses: Asiful Arefeen, College of Health Solutions, Arizona State University, 6161 E Mayo Blvd., Phoenix, AZ 85054, USA, aarefeen@asu.edu; Ali Akbari, Department of Biomedical Engineering, Texas A&M University, 5045 Emerging Technologies Bldg, College Station, TX 77843-3120, USA, aliakbari@tamu.edu; Seyed Iman Mirzadeh, School of Electrical Engineering & Computer Science, Washington State University, 355 Spokane Street, Pullman, WA 99164-2752, USA, seyediman.mirzadeh@wsu.edu; Roozbeh Jafari, Department of Biomedical Engineering, Texas A&M University, 5045 Emerging Technologies Bldg, College Station, TX 77843-3120, USA, rjafari@tamu.edu; Behrooz A. Shirazi, School of Electrical Engineering & Computer Science, Washington State University, 305 NE Spokane Street, Pullman, WA 99163, USA, shirazi@wsu.edu; Hassan Ghasemzadeh, College of Health Solutions, Arizona State University, 6161 E Mayo Blvd., Phoenix, AZ 85054, USA, hassan.ghasemzadeh@asu.edu.

2637-8051/2021/7-ART111 $15.00
https://doi.org/10.1145/1122445.1122456

1 INTRODUCTION

CVDs have been a major concern for human health for a long time and touted as the leading cause of death [15]. World Health Organization (WHO) declared that CVDs were responsible for the death of almost 17.9 million people in 2016 - 31% of all global deaths. 85% of these deaths are due to heart attack and stroke [57]. CVDs can also cause permanent or temporary disabilities and reduce the quality of life [33]. As a consequence, numerous research in CVD diagnosis have been carried out for the past decades with the goal of preventing and managing cardiac diseases [31, 34]. For in-time CVD diagnosis, it is vital to contentiously monitor HRV parameters that requires accurate estimation of IBI [1, 18].

IBI is one of the most important parameters that can be extracted from ECG and photoplethysmography (PPG) signals. IBI in an ECG signal is the time interval between two consecutive beats as shown in Figure 1 and generally measured in units of milliseconds. In normal heart function, each IBI value varies from beat to beat. This natural variation is known as HRV. However, certain cardiac conditions may cause individual IBI values to become nearly constant, resulting in lower HRV values. This can happen, for example, during periods of exercise as the heart rate (HR) increases and the beats become more regular. Certain illnesses can cause the HR to increase and become uniform as well, such as when a subject is afflicted by an infection. In fact, IBI and HRV can be used as indicators of degraded cardiac system and can be early indicator of certain cardiac diseases [13].

Wearable sensors provide an opportunity for continuous and convenient measurement of health parameters such as IBI. For the last decade, there has been immense development in the domain of wearable devices for physiological parameter monitoring, disease diagnosis and early prevention. Sleep apnea monitoring [10, 55], cardiac anomalies or arrhythmia detection/classification [19, 22, 41], HRV estimation [37], ECG monitoring [58], diabetes monitoring [6], gait assessment [32], edema monitoring [14], activity recognition [47, 49], dietary intake assessment [20], and stress monitoring [21, 50] are some of the tasks worth mentioning.

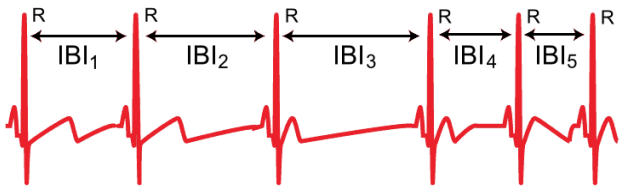

Fig. 1. R-R interval or IBI in an ECG.

Although PPG sensors embedded in various wearables such as smart watches and smart rings enable conventional, convenient and continuous measurement of IBI, processing PPG and extracting IBI values from them is challenging due to their noise susceptibility. PPG sensors are particularly sensitive to noise and human hands have a higher degree of freedom and therefore exhibit more motions than the chest [5] leading to noisy signals. ECG, as opposed to PPG, includes more information about human heart activity. Alongside other tests, ECG is frequently used to diagnose and monitor conditions affecting regular activities of heart. Regardless of the intensity and type of motion, ECG is also prone to power-line interference and Gaussian noise [29] which sometimes distort the morphological features and curb diagnosis process. Denoising ECG and recovering the fiducial points can provide extra value because diagnosis of arrhythmia is highly dependent of the shape of ECG. Thus, being able to remove noise from ECG, in general, is essential.

ECG signal that is embedded with Gaussian out-of-band noise can be denoised easily using different types of finite impulse response (FIR) filters and empirical mode decomposition (EMD) techniques [11]. However, an ECG signal that is corrupted with motion artifacts cannot be dealt with ease as the frequency spectrum of some of

these noises (1-10 Hz) [27] overlaps with those of the PQRST contents (0-50 Hz) [28, 54]. Such situations emerge specially when the subject is in constant and/or periodic motion or performs exercise, where extracting IBI values from these motion embedded ECG signals is critical. Even if IBI is directly estimated under mobility, it will be nowhere near perfect. Therefore, there is an unmet need for noise rejection techniques that can deal with the high level of noise and motion artifact.

To overcome aforementioned unmet need, we propose a novel framework to determine IBI values from ECG signals totally buried in intense motion artifact noise. We have modified *The One Hundred Layers Tiramisu* network [24], made it suitable for time-series denoising process, and used it for our case. While the original Tiramisu model in [24] had hundred convolution layers with a crossentropy loss function appropriate for classification tasks, the one in our proposal is tailored lightweight with fifty convolution layers followed by a mean squared error (MSE) loss function. The intention of this study is to eliminate motion artifact and make the R-peaks of an ECG signal more prominent in a way that IBI values can be estimated from it as accurately as possible. Our modified network works as an autoencoder. Autoencoder is a well-known framework for making compact representation of a signal and taking it back to its original dimensions if required. Our methodology intends to squeeze the given ECG signal using autoencoder, suppress the noise, get back to the original dimensions, and represent the ECG signal with its peaks sufficiently visible to calculate IBI values. The autoencoder used in this experiment is comprised of fully convolutional dense networks (FC DenseNet) - a Tiramisu model - which is familiar for image segmentation, image classification and more recently time domain analysis.

In the process of estimating IBI values from noisy ECGs, the contribution of this paper can be highlighted as follows.

1. An FC DenseNet based deep learning approach - derived from *The One Hundred Layers Tiramisu model* [24] - which performs as a robust autoencoder to suppress the noise and makes the R-peaks of the noisy ECG signal more notable. To the best of our knowledge, such a stacked tiramisu model is yet to be applied on ECG with intense noise and IBI estimation as well.
2. Our proposed methodology is capable of reckoning IBI values from ECG with noise level up to -30dB with a considerable error of 13 milliseconds (RMSE). Thus far, we have not identified other studies going beyond -30dB without the inclusion of high frequency or Gaussian white noise which are easy to eliminate using FIR filters.

As established by the tiramisu model in [24], our proposed approach does not require any sort of pre-processing or post-processing algorithms or tools in contrast to many concurrent studies. However, a simple peak picking algorithm has been used to facilitate the IBI calculation procedure.

The remaining of this paper is organized as follows. Related works are discussed in Section 2. The dataset used in this work, noise signals, their characteristics, and noise addition protocols are discussed in Section 3, development of the proposed method is explained in Section 4, results, detailed comparison with state of the art work in Section 5, observations, drawbacks, and discussions are presented in Section 6. In the end, we conclude with a brief conclusion in Section 7.

2 RELATED WORK

Research in the field of IBI estimation and ECG R-peak detection, which is a requirement for IBI estimation from noisy ECG, is extensive. Researchers have used a plethora of signal processing tools and techniques for accurate estimation of IBI in presence of motion artifacts. Mostly, they have focused on some publicly available ECG datasets like MIT-BIH Arrhythmia database or IEEE SP Cup Dataset (2015).

Removing high frequency noise or Gaussian noise from ECG and then estimating IBI from it can be achieved by applying straightforward moving average [39], low-pass, high-pass or band-pass FIR filters [2, 43], Empirical Mode Decomposition (EMD) technique [26, 53], Pan-Tompkins peak detection [38], and wavelet transformation

[51]. However, the challenge starts when we tend to do the same in presence of heavy motion artifacts. Again, baseline wander and power line noise can be removed by using band-pass filter and notch filter. But, electrode motion artifact noise - which is caused by skin stretching and alters the impedance of the skin around the electrode - takes rigorous process to be encountered as its frequency spectrum (1 to 10 Hz) overlaps with that of the PQRST complex of ECG waveform [27].

Rahel et al. designed a study to evaluate the IBI signal qualities of a Holter device and a heart rate chest belt monitor while the subjects were at rest and were performing 5 different levels of activities like sitting and reading, doing household chores, walking, jogging, and training [16]. But there is no indication of the specific amount of noise they dealt with. *Shalini et al.* used Slope Sum Function and Teager-Kaiser Energy operator method for R-peak artifacts detection in cardiovascular and non-cardiovascular signals like Electroencephalogram (EEG), Electrooculogram (EOG), and Electromyogram (EMG) [44]. However, they too didn't mention the SNR level up to which their algorithm works perfectly.

Sonia et al. discussed a new time delay estimation technique which is essentially derived from operational calculus, differential algebra, and non commutative algebra and helps to estimate RR interval from noisy ECG with SNR level up to 6dB with a considerable number of false peak detections [46]. *Aygun et al.* proposed a technique to select the fiducial points from noisy ECG and PPG signal using shortest path algorithm which takes the advantage of time-continuity of heartbeats [9]. With this, they accurately measured IBI up to -2dB SNR level which they later used for determining HRV [8]. Here, the derivatives of the ECG or PPG signal are calculated using Savitzky-Golay method to detect the possible fiducial points like R-peaks, systolic peaks, points with maximum slope, and onset points. Since the signals are noisy, they ended up getting too many candidate points and most of them were false fiducial points if not all. With all these points, a graph was generated for each signal where the edges refer to IBIs, both true and false IBIs, and the vertices refer to morphological points, also both true and false. From this graph, it was clear that the starting point of one heartbeat is the end point of the last one and there is no disruption between them. Any candidate path that satisfies certain conditions derived from average HR can be considered as a true IBI and the two associated nodes/vertices as true morphological point for that specific signal. Next, each of the vertices were connected to some previous vertices which fell within a specific time window. If the time difference between the reference vertex and any neighboring vertex deviated the average IBI (which was calculated using average HR), the corresponding edge i.e. the 'time interval' was assigned zero weight. Otherwise, a numerical weight was assigned to it where the weight varied according to its difference with the average IBI. The intuition behind this weighting is the fact that the true IBIs should remain close to the average IBI calculated from the average HR. The weights of the vertices were also derived from the weights of corresponding edges. After all these weight distribution, the vertex with the minimum accumulated weight, is the chosen true vertex inside the time window. This is indeed leveraging the shortest path algorithm and enables detecting the IBIs that are closest to the average IBI. Finally, they combined all the shortest paths and formed an array for each of the morphological features of each ECG and PPG signal. An overview of this process is depicted in Figure 2. Although both [8] and [46] have employed novel mathematical tools for IBI estimation without necessarily denoising the entire ECG signal, they haven't been able to go far in terms of SNR level.

Many researchers have focused on R-peak detection from noisy ECG signals. As mentioned earlier, a robust peak detection algorithm can also lead to accurate IBI estimation. In addition to applying a band-pass filter for removing power line and baseline shifting noise, *Pulavskyi et al.* performed a two-stage smoothing using the 'boxcar' and 'parzen' kernel. This methodology allowed them to detect peaks with good precision and recall values up to -15dB, however, there was presence of white and pink noise which decreased the relative weight of electrode motion and muscle artifacts [40].

With advanced deep learning mechanisms, denoising tasks have gone further as they have been able to obtain higher accuracy with minimal human supervision. To talk about a few deep learning based approaches, *Ansari et al.* exploited a simple convolutional neural network (CNN) to differentiate between usable and unusable ECG

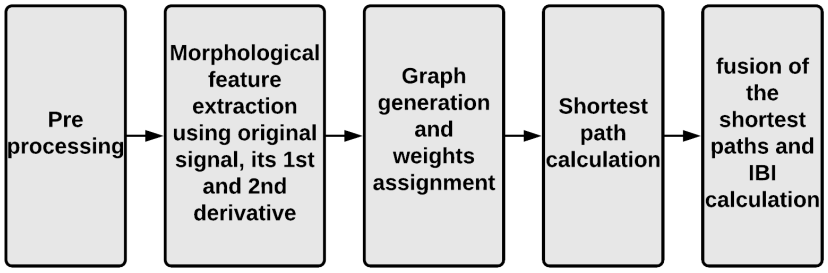

Fig. 2. Overview of the work presented by *Aygun et al.* [8].

segments. The usable segments have higher probability of QRS detection. They carried out their research up to 0dB with some error [3]. *Juho et al.*, on the other hand, utilized a bidirectional Long-Short Term Memory (LSTM) network to suppress the noise up to 0.1dB and detect peaks from it [30]. A CNN encoder-decoder is used by *Natasa et al.* to denoise the QRS complexes of the long term ECG signals acquired with their wearable armband device and used them later to calculate HR [45]. They too were able to use the denoising process up to -17dB with inclusion of white and brown noise, but no muscle artifact. *Sricharan et al.* modified the conventional U-Net [48] algorithm for time-series data and used it along with distance transformation to determine the position of the ECG R-peaks for noise level up to 0dB [56]. The peak detection task was framed as a regression task in [56]. They obtained the Distance Transformation (DT) of all the ECG signals which disclose the distance of each point on the ECG from its nearest peak. It results in a zig-zag wave where the lowest points refer to the R-peaks of the corresponding ECG signal. The DT is of the same size as its input ECG. They have exploited the U-Net architecture with conventional encoder-decoder where the encoder performs downsampling with 8 layers of strided-convolutions, the decoder does upsampling in a similar way but in opposite direction. Both the encoder and decoder perform 1D convolution and there is a bottleneck between them to hold the minimum representation. Additionally, a residual inception block was placed at each layer which exploits skip connections to discard vanishing gradient problem and ensure fast convergence. The architecture for this work is illustrated in Figure 3.

Likewise, *Lishen et al.* took advantage of U-Net and DR-Net to successfully perform a two-stage denoising process [42]. *Karol* designed a generative adversarial network (GAN) based ECG synthesizer to generate a synthesized ECG dataset. Later, noise was added to the artificial ECG, and a CNN autoencoder was trained using this dataset to achieve an MSE of 0.017 (direct from the optimizer during training) [4]. Finally, *Brosnan et al.* [59] demonstrated peak detection with a machine learning pipeline consisting of a Butterworth filter, two wavelet convolutional neural networks (WaveletCNNs) autoencoders, an optional QRS complex inverter, a Monte Carlo k-nearest neighbors (k-NN), and a convolutional long short-term memory (ConvLSTM) as shown in Figure 4.

The noisy one-channel ECG signal is fed into the Butterworth filter with a cut-off frequency set at 5Hz to remove baseline shifting noise by attenuating the low-frequency components. Next, the output is decomposed using symlet-4 wavelet to obtain the wavelet coefficients. These coefficients are then fed into a CNN autoencoder, where the noisy unnecessary coefficients are rejected, but the significant parts are retained, producing clean wavelet coefficients that are significant for further analysis. The CNN autoencoder that takes on the wavelet coefficients has a 2-layered encoder, a bottleneck, and a 2-layered decoder, with a Leaky-ReLU activation layer at each hidden layer. A wavelet reconstruction is performed to get the coefficients back to the original form, i.e., a single-channel ECG. After that, a difference filter is deployed prior to the next wavelet autoencoder to refine the QRS complexes by suppressing the low-frequency components. The signal is then passed to the second wavelet autoencoder, which has the same functionality as the previous one. Both of these wavelet autoencoders work as

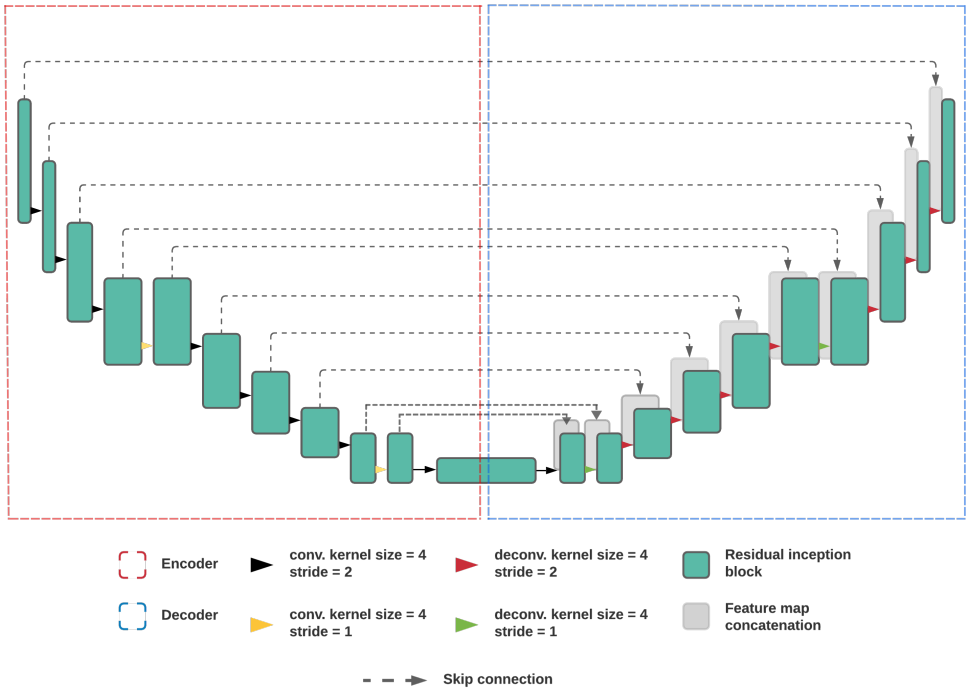

Fig. 3. The U-Net architecture used by *Sricharan et al.* [56].

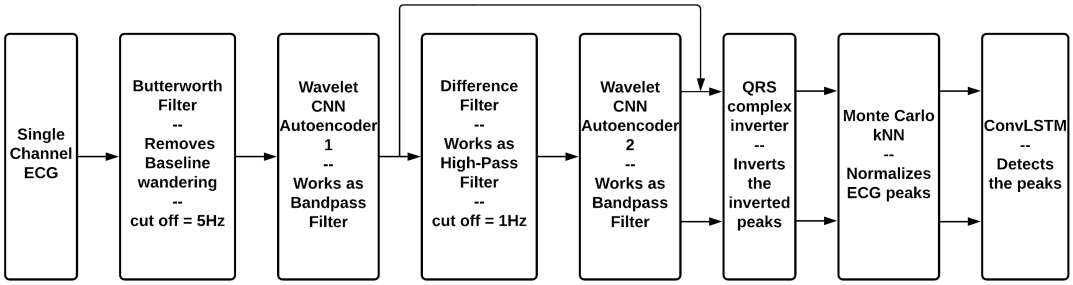

Fig. 4. The machine learning pipeline developed by *Brosnan et al.* [59].

bandpass filters to remove unnecessary components. To deal with the inverted peaks, an inverter was placed right after the second autoencoder, and it simply inverted the already inverted peaks. Then, the Monte Carlo k-NN method was utilized to normalize the ECGs by scaling the beats to unit millivolt. Finally, the ConvLSTM network was applied to detect the peak points, as it has pattern matching ability to detect specific characteristics from a time-series signal. They used the MIT-BIH, the European ST-T, and the Long Term ST database Noise Stress Test databases, going up to -6dB, and recorded some good results. However, all these deep learning-based methods failed to leverage different deep learning algorithms' power to improve the denoising accuracy or IBI estimation and explore intense noise scenarios.

Table 1. List of used ECG recordings from different databases.

MIT-BIH Arrhythmia Database		European ST-T Database	IEEE SP Cup 2015
Train data		Train data	Train data
100	102	e0103	1
		e0104	5
Test data		Test data	Test data
101	209	e0105	2
103	213	e0106	3
109	219	e0107	4
112	220	e0113	6
113	223	e0114	7
115	228	e0115	8
116	230	e0118	9
122	231	e0122	10
123	234	e0123	11
		e0126	12
		e0127	
		e0129	

3 DATASETS

We have opted to use clean ECG recordings from publicly available databases like MIT-BIH Arrhythmia Database v1.0.0 [17, 35], European ST-T Database from PhysioNet [52], and IEEE Signal Processing Cup 2015 [60].

The sampling frequency of the MIT-BIH Arrhythmia Database is 360 Hz, i.e., 1 sample in every 2.78 ms. For ease of calculation and noise addition, we upsampled both the European ST-T Database and the IEEE SP Cup 2015 dataset from 250 Hz and 125 Hz to 360 Hz, respectively.

Next, we added electrode motion (EM) noise, motion artifact (MA) noise, and baseline wandering (BW) noise from the MIT-BIH Noise Stress Test (NST) Database v1.0.0 [36] and generated noisy data for different SNR levels, starting from 36dB to -36dB with a decrement of 6dB. Therefore, for each clean ECG signal, we generated 13 variants with different SNR levels. Needless to mention, noise was added to the signals thoroughly instead of adding them between consecutive rest periods. Noise addition was carried out following the standard approach [42] in the NST Database:

$$ECG_{\text{noisy}} = ECG_{\text{clean}} + [a_1] * EM + [a_2] * MA + [a_3] * BW$$

Where ECG_{clean} refers to the clean ECG signal and a_1, a_2, a_3 gain values are adjusted according to the expected SNR value. Since we are more interested in estimating IBI values from a signal totally buried under muscle artifact and electrode motion, these two noises have been assigned higher weights, meaning $a_2 > a_1 > a_3$. The noise recordings were produced with physically active volunteers and captured with conventional ECG recorders, leads, and electrodes; the electrodes were positioned on individuals' limbs in areas where the ECGs could not intervene. The noise signals were recorded for half an hour, and the volunteers were in light motion during the collection phase. Thus, they are not synthetic but real.

In this work, we used the first 409600 data points of each ECG signal since the noise signals have limited data points. Figure 5 shows a clean segment of ECG data from the MIT-BIH Arrhythmia database (recording # 101) and its corresponding noisy variants starting from 6dB to -36dB. As the noise increases, specifically after 0 dB, the R-peaks become heavily buried in noise, and detecting them with conventional signal processing techniques would be very inaccurate and challenging, if even possible. These artifacts enforce redundant tests, additional costs, and sometimes require specialists' intervention. Table 1 lists the recordings from different datasets used for training and testing. The training set was selected at random. However, distorted signals and ECGs with

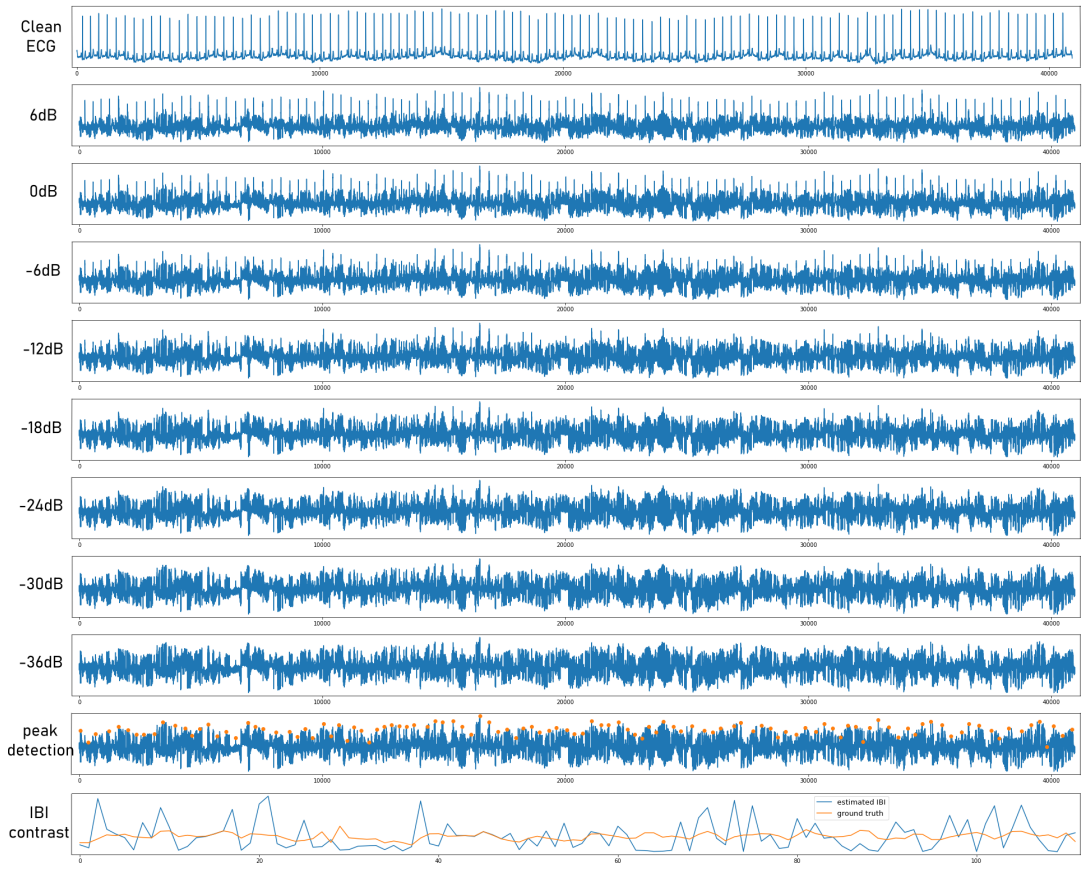

Fig. 5. A clean ECG segment and its noisy variants. EM, MA, BW noises have been added to clean signals and the numbers on the left of each box refer to corresponding SNR values. IBIs estimated from raw and noisy ECG signal are highly inaccurate compared to the true IBIs.

missing peaks were not included in the training of the model. Usually, autoencoder-type models require very small training data [56], and our case is no different.

4 PROPOSED METHODOLOGY

Our working principle starts with a fully convolutional-dense deep neural network (tiramisu model) [24]. Noisy signals are fed to this model which has multiple convolution and pooling layers intuitively responsible for compressing the signal to a smaller representation, eliminating the noise, retaining the most patterned and prominent features, and making the peaks more visible. Later, we identify the peaks with a simple peak picking algorithm and then calculate IBI values from there. The overall procedure of this work is illustrated in Figure 6.

4.1 Tiramisu Model

Calculating IBI values from noisy ECG readings is challenging. As a potential solution, transformers/autoencoders are well-known architectures used for minimizing the difference between the input and output, such as denoising.

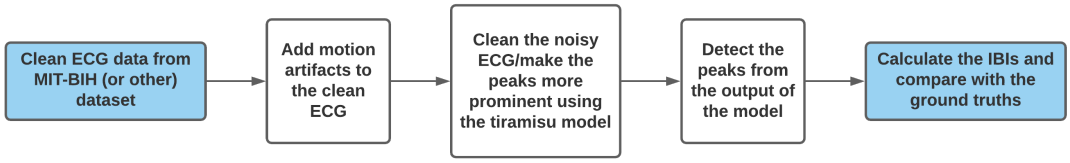

Fig. 6. An overview of the proposed IBI estimation framework.

This means that the objective function of any such architecture is focused on producing results ($\hat{x}$) similar to the input (x) i.e.

$$\min |x - \hat{x}| \tag{1}$$

Hence, we designed a robust tiramisu model - a member of the autoenoder family - which consists of stacked dense blocks (DB) and numerous feedback loops. High number of dense blocks and feedback loops eliminate the requirement of pre-processing as the model itself is capable of removing high frequency or Gaussian white noise. While the convolution and pooling layers perform the job of squeezing out the noise, the skip connections between layers allow the output of each dense block and up convolution to encode finer details from actual signal and later layers, solve the gradient vanishing problem, and provide improved results than without them. In contrast to the standard U-Net architecture, the dense blocks in the tiramisu model have skip connections within themselves which eliminate the possibility of gradient vanishing within the contraction path.

The overall architecture of the proposed model is illustrated in Figure 7. As depicted, the model incorporates a contraction path, a bottleneck, an expanding path, and certain skip connections. The skip connections here help the expanding path (or upsampling path) to get back information from the contraction path, reuse them and thus abolish gradient vanishing. The main theme of this model is to take advantage of feature reuse and take the already complicated DenseNet a step ahead.

The contraction path (or downsampling path) starts with a convolution with kernel size = 3. Then comes a series of consecutive dense blocks and transition down (TD) blocks. Prior to the bottleneck, 3 dense blocks have been placed on the contraction path with each having 4, 5, and 7 layers respectively. Right after each dense block, a TD block has been attached. Note that, the TD blocks perform the pooling operation and cause some information loss and resolution reduction along the downsampling path. In between, there are concatenation blocks to create feedback loops from previous layers.

The expanding path is almost a mirror symmetry of the contraction path except it has lesser feedback loops and the TD blocks are replaced by transition up (TU) blocks along the path. These TU blocks does transposed convolution operation and upsample the previous mappings. The upsampled mappings are then concatenated to the mappings coming from the downsampling path via skip connections and form a new input for the next dense blocks along expanding path. The last dense block in this trajectory sums up the information from all the previous dense blocks. Unlike the contraction path, we do not concatenate the input of a dense block with its output since it does not make any significant difference. The final convolution in this path is done with window size = 3. The dense block that lies between these two paths is the bottleneck.

The dense blocks in the model have different number of layers which perform one dimensional convolution with kernel size = 3, *ReLU* activation function, Batch Normalization, and drop out value of 0.2. The batch normalization function is given by-

$$BN(x) = \frac{x - \mu_x}{\sigma_x} \tag{2}$$

where, μ_x is the mean and σ_x is the standard deviation of input matrix x.

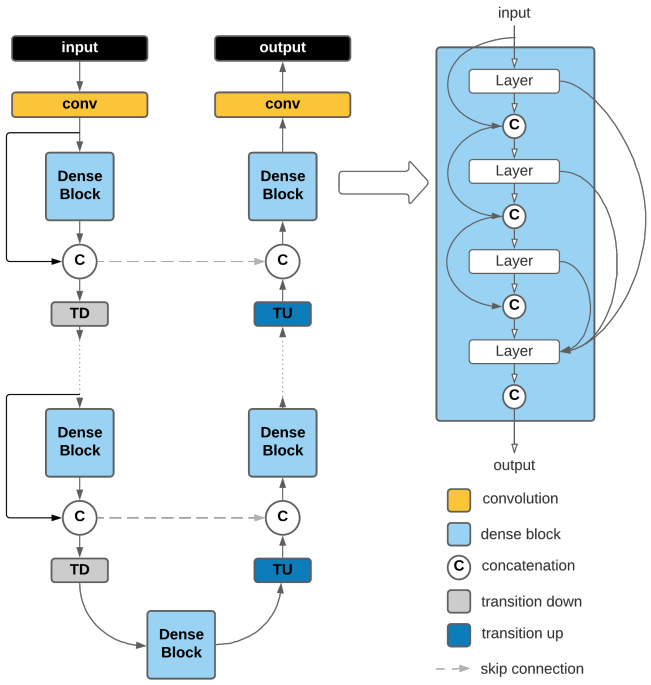

Fig. 7. Big picture view of the proposed model. It consists of a contraction and an expanding path. Both paths have several convolution blocks, dense blocks, transition downs, transition ups, concatenations and skip connections. The dense block between these two paths is the bottleneck.

The TD layers also use one dimensional convolution with kernel size = 1, *ReLU* activation, Batch Normalization, drop out value of 0.2 and Max Pooling with pool size = 2. However, the TU layers execute transposed convolution with kernel size = 3 and stride = 2.

We have employed *tanh* activation on the final output layer to ensure that the output is between [-1 1] and to gain non-linearity for better advantage during derivative calculation. The *tanh* function can be written as-

$$tanh(x) = \frac{e^{x} - e^{-x}}{e^{x} + e^{-x}} \tag{3}$$

As mentioned earlier, 3 dense blocks have been employed on either path with each block having 4, 5, and 7 layers respectively. Also, the architecture has 3 TUs or TDs and 1 input or output block on either side. Since each layer has one convolution layer, each TU or TD also perform one convolution and each input/output block has one convolution layer, There are a total of 40 convolution layers in the contraction and expanding paths combined. Additionally, the bottle neck dense block has 10 layers i.e. 10 convolution layers. Summing up, a total of 50 convolutions are done in this entire model. All the convolutions (except last one) are equipped with *ReLU* activation, L2 regularization with factor of 0.01 and zero padding for redeeming the initial shape. Finally, Adam optimizer with a default learning rate of 0.001 has been used followed by a mean square error (MSE) based loss function-

$$MSE = \frac{1}{N}\sum_{i=1}^{N}(y_i - y_i^p)^2 \tag{4}$$

Table 2. Tiramisu model architecture and contents of layer, TD and TU blocks.

Full tiramisu model architecture
Input
Convolution: kernel size = 3
DB (4 layers) + TD
DB (5 layers) + TD
DB (7 layers) + TD
Bottleneck: DB (10 layers)
DB (7 layers) + TU
DB (5 layers) + TU
DB (4 layers) + TU
Convolution: kernel size = 3
tanh activation
Output

Layer block	**Transition Down (TD) block**	**Transition Up (TU) block**
Batch Normalization	Batch Normalization	Trans. convolution: kernel size = 3
ReLU activation	*ReLU* activation	l2 regularizer (0.01)
l2 regularizer (0.01)	l2 regularizer (0.01)	*stride* = 2
Convolution: kernel size = 3	Convolution: kernel size = 1	
Dropout p = 0.2	Dropout p = 0.2	
	Max Pooling: size = 2	

where, y_i and y_i^p refer to actual target values from ground truth sequences (noise free ECG) and predicted values from recovered sequences respectively and N is the number of data points.

The model have been trained for one hundred iterations without any early stopping criteria while a batch size of 16 have been maintained throughout the entire experiment. 80/20 ratio has been chosen for train/validation split.

Table 2 shows the full architecture of our tiramisu model and the constituents of layer, TD, and TU blocks.

4.2 Peak Detection

Although numerous peak picking algorithms can be found in the literature [23], our choice is a generalized algorithm [25]. Usually, resting HR varies from 60-100 bpm [7]. But for athletes, it could be as low as 40 bpm during rest periods and as high as 200 bpm during work out sessions [12]. Our sampling frequency is 360 Hz. It ensures that there must be at least one beat in every 108 to 540 data points. Therefore, we have used an algorithm that takes on a given signal and finds out all the local maxima which must be at least 108 data points apart from each other. In this way, we may end up getting some false peaks because, when the noise is intense and a motion artifact-induced peak is higher than its neighboring R-peak, the tiramisu model fails to detect the R-peak and removes it while the motion artifact remains. Subsequently, the peak detection algorithm detects this motion artifact as an R-peak causing some error.

4.3 IBI Calculation

Under any circumstance, to estimate IBI precisely, the position of the beats/peaks need to be detected accurately. After denoising the signal using the proposed AE-based model and detecting the R-peaks, in this step, the IBI value using the identified R-peaks can be extracted with Equation 5.

$$IBI_i = t_i - t_{i-1} \tag{5}$$

where, t_i is the occurrence time of the i^{th} R-peak and IBI is extracted for all peaks in an ECG signal.

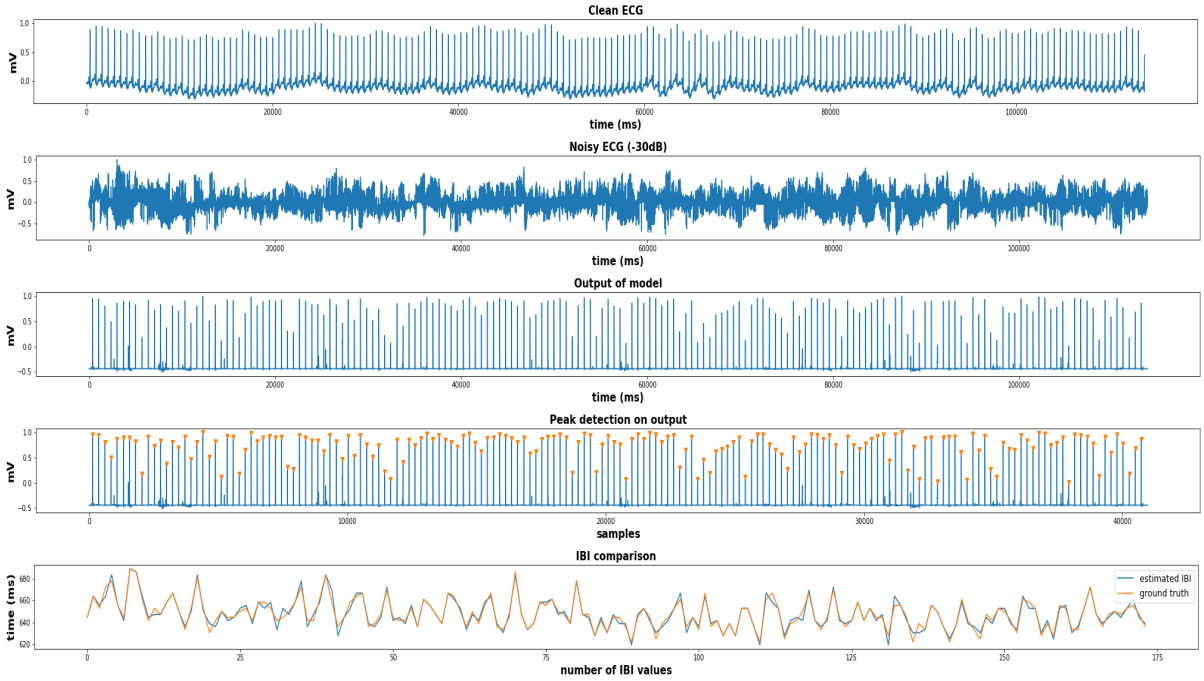

Fig. 8. ***Clean ECG:*** An ECG segment from MIT-BIH Arrhythmia Database (recording # 234). ***Noisy ECG:*** Muscle artifact, baseline wander and electrode motion noise have been added to the clean signal. Resulting SNR of the ECG is -30dB. ***Model output:*** The noisy ECG is fed to the tiramisu model and the output has the R-peaks more prominent. ***Peak Detection:*** Peak detection algorithm has been applied to the output. ***IBI Comparison:*** IBI values estimated from the prominent peaks and compared against the ground truth IBI values. The RMSE of IBI values in this case is only 3.44 ms.

5 RESULTS

In this study, the aim is to make the R-peaks of noisy ECG more prominent to estimate IBI from it as accurately as possible. We evaluate the performance of our approach by testing it on different levels of noisy ECG, which have been generated by adding certain level of noise, explained in Section 3. In this section, we define our evaluation metrics and measure the performance of our model in terms of estimated IBI values extracted from ECGs with different SNR levels. Lastly, we will compare our approach against a few state-of-the-art methods designed for IBI calculation and/or peak detection from noisy ECG.

For further explanation we refer to Figure 8. The clean ECG in this figure is the first 40960 data points of recording 234 from MIT-BIH Arrhythmia Database. Three different noises have been added to the clean ECG to get a noisy signal of -30dB SNR. -30dB refers to a very high amount of noise and implies that the power of noise is 10^3 times that of actual signal. Without any pre-processing, this noisy ECG is then fed to the tiramisu model to make the R-peaks more visible. Next, our peak detection algorithm has been applied to the output of the model. We estimated IBI values from the beats and in the final box, we have compared our IBI values with that of the ground truth and recorded an RMSE of 3.44 ms.

Prior studies in the field of ECG denoising and beat detection exercised SNR_{imp}, *Sensitivity* or F_1 *score* to evaluate their performance regarding detecting correct peaks. However, herein, we are interested in estimating

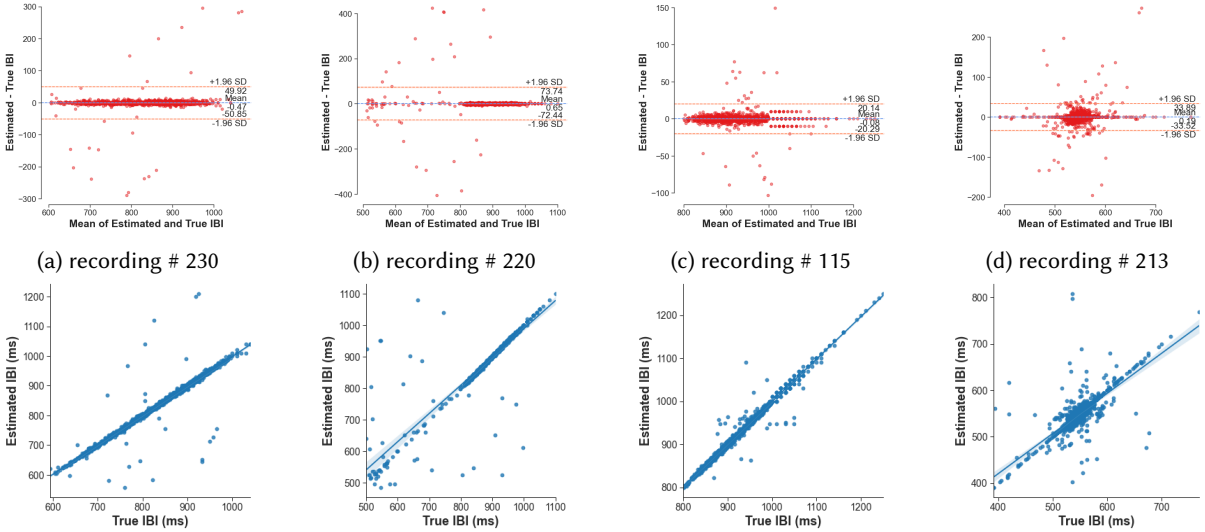

(a) recording # 230 (b) recording # 220 (c) recording # 115 (d) recording # 213

(e) recording # 230 r = 0.9595 (f) recording # 220 r = 0.9273 (g) recording # 115 r = 0.9895 (h) recording # 213 r = 0.9006

Fig. 9. Bland-Altman plot with LOAs are depicted in Figs. 9a to 9d for different recordings. Also, correlation plot for same recordings are shown with Pearson correlation coefficient in Figs. 9e to 9h. For some ECGs, the proposed method achieves r values like 0.9895 though nominal values like 0.9 also exist.

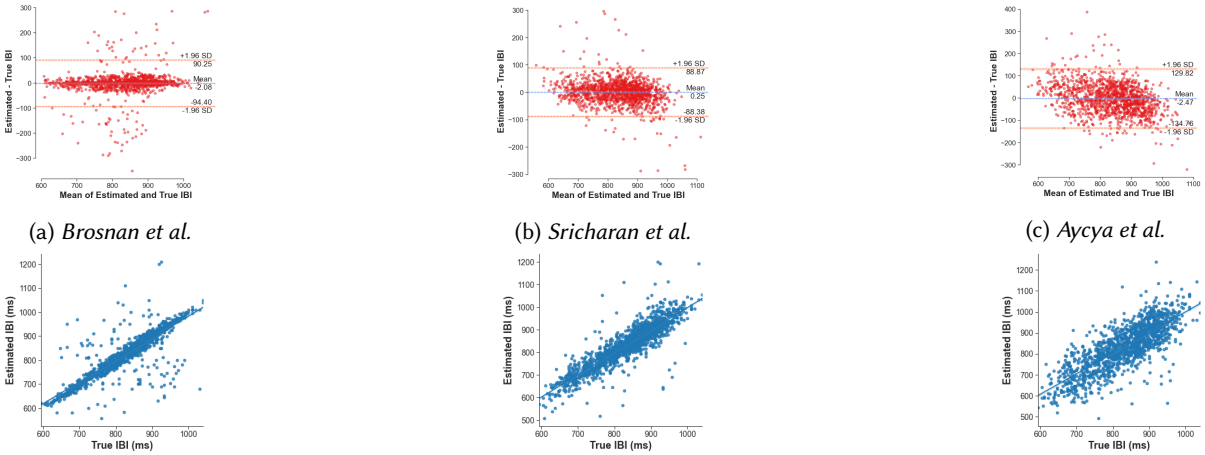

(a) *Brosnan et al.* (b) *Sricharan et al.* (c) *Aycya et al.*

(d) *Brosnan et al.* r = 0.8883 (e) *Sricharan et al.* r = 0.8663 (f) *Aycya et al.* r = 0.7897

Fig. 10. Bland-Altman plot for IBI estimation on recording # 230 using methods of *Brosnan et al.*, *Sricharan et al.*, and *Aycya et al.* are depicted in Figs. 10a to 10c respectively. Corresponding correlation plots are also shown along with correlation coefficients in Figs. 10d to 10f.

IBI from noisy signals. Therefore, we selected our performance metrics based on that objective and leveraged *RMSE* and *% error* of IBI for performance evaluation. We define those metrics as follows-

$$\text{RMSE}_{IBI} = \sqrt{\frac{\sum_{i=1}^{n}(P_i - O_i)^2}{n}} \tag{6}$$

$$\%error = \frac{1}{n}\sum_{i=1}^{n}\frac{|O_i - P_i|}{O_i} \times 100\% \tag{7}$$

where, P_i refers to predicted IBI, O_i denotes observed IBI (groundtruth), and n indicates number of IBIs in one segment of ECG. As shown in Figure 8, the denoising algorithm performs very good at exposing the R-peaks. On top of that, the peak picking algorithm has also performed well to detect the exposed peaks. The peak picking algorithm has found extra peaks (false peaks) in the recovered signals from -30dB SNR on extremely rare occasions, with an approximate average ratio of 120:1. Given the fact that these false peaks are in between true peaks and incur very small error in IBI estimation, their presence is simply ignored in evaluation.

The Bland-Altman plots in Figs. 9a to 9d show comparison of the IBIs estimated from noisy ECGs of SNR -30dB against their true IBIs. The ECGs considered in these plots are recordings # 230, 220, 115 and 213. The limits of agreements (LOAs) - which work as boundary for 95% of data and a good measurement of accuracy - are located at [49.92, -50.85] ms, [73.74, -72.44] ms, [20.14, -20.29] ms, and [33.89, -33.52] ms respectively. Also, the Pearson correlation plots are illustrated in figs. 9e to 9h for the same set of recordings. The high correlation coefficients (r) - 0.96, 0.93, 0.99, and 0.9 - emphasize that the estimated IBIs are very coherent to the true IBIs.

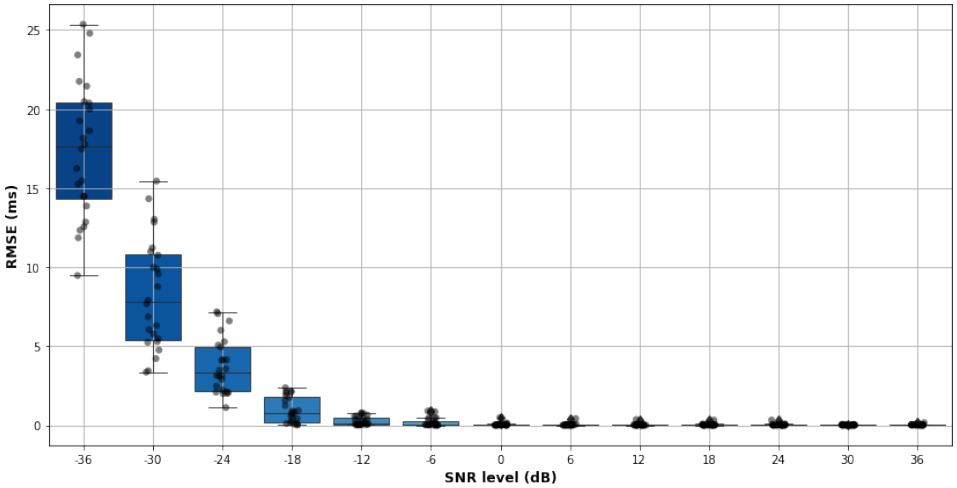

Fig. 11. Box and whisker plot for different SNR levels of test data of MIT-BIH Arrhythmia Database. On the x-axis we have SNR values starting from 36dB up to -36dB and on y-axis RMSE (ms) values are listed. The RMSEs are calculated by comparing the estimated IBIs with the true ones. Circular dots with low opacity are different RMSE values. The horizontal edges of colored boxes mark the interquartile range (IQR) (Q_1-Q_3) and contain 50% data whereas the black horizontal lines inside each box mark the median value. The vertical whiskers hold other 50% of the data and black horizontal lines mark the minimum and maximum. ♦ symbols are the outliers.

In comparison, similar plots are also shown in figs. 10a to 10c and figs. 10d to 10f highlighting the performance of *Brosnan et al.*, *Sricharan et al.*, and *Aygun et al.* respectively on recording # 230. The LOAs are at [90.25, -94.40] ms, [88.87, -88.38] ms, and [129.829, -134.76] ms respectively. Thus, our method is ensuring [40.33, -43.55] ms, [38.95, -37.53] ms, and [79.91, -83.91] ms of improvements respectively. As stated in corresponding papers, these methods also perform well under low noise situations. Correlation coefficients (r) for these methods on this specific recording are 0.88, 0.87, and 0.79 respectively whereas our approach obtains 0.96 correlation for the same setting. For other recordings of same dataset, none of these 3 methods achieve correlation above 0.9 at an SNR value of -30dB. Performance of all methods (including ours) decline for recordings of IEEE SP Cup 2015 and European ST-T Database and the rationale has been clearly explained in Section 6.

The accuracy of the proposed methodology can also be inferred from the box and whisker plot depicted in Figure 11. The IBI values have been estimated for all 13 noisy variants of the test ECGs in MIT-BIH Arrhythmia Database listed in Table 1 and compared with that of the clean versions. Notice that, we hardly get any error for SNR values up to -12dB and the estimated IBI values are consistent and nearly as good as the true IBIs. However, starting from -18dB, we encounter some amount of error and above -30dB the noise becomes very intense as well as the RMSE. The median value at -30dB is 7.792 ms.

Plots of true IBIs, IBIs estimated with our approach and that of *Brosnan et al.* (both at -30dB) are pictured in Figure 12. Some other methods have not been included with a view to keeping the plots clean to understand. IBIs estimated with our approach are not that much different from the true one following the trend in a cogent way.

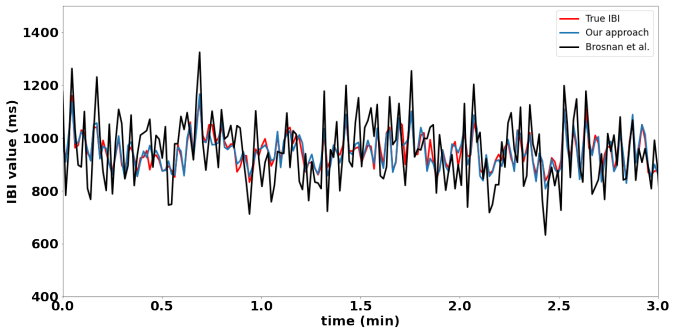

Fig. 12. Comparison of IBI plot with true IBIs and estimated IBIs obtained by *Brosnan et al.*. For higher resolution, only first 3 minutes have been plotted.

Lastly, we preform comparative analysis of 3 state-of-ther-art and our proposed method on MIT-BIH Arrhythmia Database v1.0.0, European ST-T Database, and IEEE Signal Processing Cup 2015 in Tables 3a to 3c (the details of these methods are described in Section 2). Once more, the performance metrics are average RMSE and average % error and noise has been added to all the signals from each dataset. In these tables we have considered SNR levels starting from 0dB to -30dB since performance of all methods on higher quality signals are almost flawless. The weighted average of RMSE is 13.514 ms and % error is 7.97% for the proposed method whereas they are 31.467 ms (17.953 ms higher than us) and 17.384% (9.414% higher) for *Brosnan et al.*, 45.439 ms (31.925 ms higher) and 23.72% (15.75% higher) for *Sricharan et al.*, 49.739 ms (36.225 ms higher) and 20.349% (12.379% higher) for *Aygun et al.*.

6 DISCUSSION

While analyzing the proposed method's performance, we have come across some of the observations, facts, and limitations which are worth mentioning-

	0dB	-6dB	-12dB	-18dB	-24dB	-30dB
Brosnan et al.[59]	1.69 ms 2.38%	6.86 ms 6.97%	15.41 ms 9.06%	21.22 ms 12.74%	28.73 ms 14.34%	31.44 ms 17.24%
Sricharan et al.[56]	2.64 ms 1.54%	8.61 ms 3.79%	12.02 ms 9.87%	20.05 ms 18.71%	49.78 ms 20.97%	54.33 ms 22.41%
Aygun et al.[8]	5.08 ms 3.54%	8.41 ms 5.88%	17.24 ms 8.77%	32.47 ms 14.27%	42.32 ms 17.31%	55.72 ms 21.83%
Proposed Method	**0.08 ms** **0.01%**	**0.17 ms** **0.08%**	**0.68 ms** **0.28%**	**1.09 ms** **0.95%**	**4.72 ms** **4.23%**	**8.39 ms** **6.34%**

(a) MIT-BIH Arrhythmia Database

	0dB	-6dB	-12dB	-18dB	-24dB	-30dB
Brosnan et al.[59]	**1.02 ms** 1.87%	**3.27 ms** **1.51%**	12.57 ms 2.59%	23.29 ms 9.61%	25.13 ms 15.02%	30.53 ms 18.72%
Sricharan et al.[56]	2.21 ms 1.21%	7.07 ms 3.17%	13.74 ms 11.51%	19.69 ms 17.94%	27.92 ms 21.38%	37.81 ms 27.33%
Aygun et al.[8]	5.32 ms 3.21%	7.95 ms 5.12%	15.33 ms 7.91%	33.41 ms 12.02%	37.97 ms 18.32%	47.86 ms 19.27%
Proposed Method	2.27 ms **0.85%**	3.85 ms 1.59%	**4.09 ms** **1.77%**	**5.76 ms** **2.31%**	**7.98 ms** **3.87%**	**10.52 ms** **7.71%**

(b) European ST-T Database

	0dB	-6dB	-12dB	-18dB	-24dB	-30dB
Brosnan et al.[59]	**2.35 ms** 2.17%	8.41 ms 4.47%	15.14 ms 7.37%	18.73 ms 9.22%	21.61 ms 13.36%	32.64 ms 16.04%
Sricharan et al.[56]	4.97 ms **1.73%**	8.82 ms 3.59%	**11.46 ms** **7.15%**	25.41 ms 15.81%	32.63 ms 17.23%	38.59 ms 21.75%
Aygun et al.[8]	6.21 ms 3.64%	**6.91 ms** **4.09%**	17.13 ms 7.42%	31.04 ms 11.90%	35.31 ms 18.47%	41.23 ms 18.98%
Proposed Method	5.14 ms 3.63%	7.11 ms 4.22%	12.16 ms 7.96%	**11.91 ms** **8.05%**	**17.84 ms** **8.79%**	**26.33 ms** **11.23%**

(c) IEEE Signal Processing Cup 2015

Table 3. Comparison of different methods on 3 dataset. For any method, the upper value refers to avg. RMSE and the lower value refers to avg. % error. Performance have been measured on signals listed in Table 1 only.

The proposed algorithm can make the peaks more visible, detect them from intense noisy signals and estimate the IBI values from it. However, it cannot redeem or rescue the typical shape of an ECG i.e. the PQRST wave. It can only recover the R-peaks.

Additionally, the IEEE SP Cup 2015 data already contains some motion artifacts, and we are adding additional noise to it. Therefore, the unexpected performance on this dataset is quite reasonable. Therefore, the subpar performance on this dataset is quite reasonable.

The performance of the proposed algorithm on the European ST-T Database and IEEE Signal Processing Cup 2015 is lower than on the MIT-BIH Arrhythmia Database, likely due to the need for upsampling the latter.

Some of the signals are not clean enough; they are missing peaks, distorted, and have some innate noise. These are beyond the scope of fixing with any sort of pre-processing, and we have had to omit such signals from the database entirely. Such a distorted signal segment is presented in Figure 13.

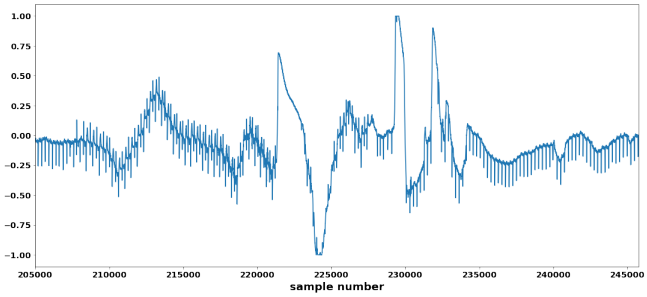

Fig. 13. A distorted ECG with missing peaks.

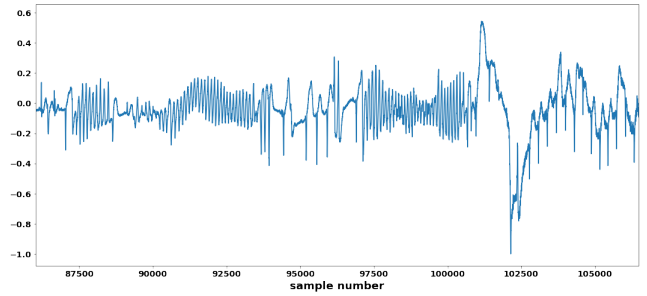

Fig. 14. An ECG with inconsistent peak size. Signals like this have been omitted in both training and testing phases since they decrease the performance.

Some of the signals have inconsistent peak sizes, like the one in Figure 14. This becomes a notable hindrance. The SNR levels are set according to the power of the ECG and power of noise. Now, in an ECG with inconsistent peak size, the consistent peaks play dominant role to set the power of ECG signal and the noise power is set accordingly. In such a case, the noise peaks adjacent to the inconsistent peaks become much higher and the tiramisu model fails to differentiate between the actual ECG peak and the noise. Consequently, it suppresses the actual peak and retains the noisy peak leading to higher error in IBI estimation.

Signals with SNR levels beyond -30dB have extremely intense noise that cannot be suppressed effectively. As a result, the detected peaks are not perfect, leading to significant errors in IBI estimation. Therefore, we claim, our method is good for estimation up to -30dB.

7 CONCLUSION

This paper presents and analyzes a novel method based on a stacked tiramisu model for extracting IBI from ECG signals submerged in motion artifacts. This method can be easily used for denoising purpose and can compete with traditional concurrent techniques. The model suppresses the noise and later, most prominent feature of ECG i.e. position of R-peaks, has been leveraged to estimate the IBIs. Also, this approach does not require any pre-processing or post-processing method which saves some of the complexities. Results show the efficiency of the proposed model and the estimated IBIs are highly correlated to that of the true IBIs even at -30dB SNR value. The weighted average RMSE for IBI estimation is 13.514 ms. Although the size of the model is massive, with tensorflowlite, it can also be optimized for embedded system applications. Our approach is generalizable, and with some slight changes, it can be adapted for denoising other physiological signals as well.

ACKNOWLEDGMENTS

This work was supported in part by the National Science Foundation, under grants CNS-1750679 and CNS-2210133. Any opinions, findings, conclusions, or recommendations expressed in this material are those of the authors and do not necessarily reflect the views of the funding organizations.

REFERENCES

[1] Mobyen Uddin Ahmed and S. Begum. 2010. Heart Rate and Inter-beat Interval Computation to Diagnose Stress Using ECG Sensor Signal.

[2] Mohammed Tali Almalchy, V. Ciobanu, and N. Popescu. 2019. Noise Removal from ECG Signal Based on Filtering Techniques. *2019 22nd International Conference on Control Systems and Computer Science (CSCS)* (2019), 176–181.

[3] S. Ansari, Jonathan Gryak, and K. Najarian. 2018. Noise Detection in Electrocardiography Signal for Robust Heart Rate Variability Analysis: A Deep Learning Approach. *2018 40th Annual International Conference of the IEEE Engineering in Medicine and Biology Society (EMBC)* (2018), 5632–5635.

[4] K. Antczak. 2020. A Generative Adversarial Approach To ECG Synthesis And Denoising. *ArXiv* abs/2009.02700 (2020).

[5] Christoph Hoog Antink, Yen Mai, Mikko Peltokangas, Steffen Leonhardt, Niku Oksala, and Antti Vehkaoja. 2021. Accuracy of heart rate variability estimated with reflective wrist-PPG in elderly vascular patients. *Scientific Reports* 11 (2021).

[6] Asiful Arefeen, Samantha N Fessler, Carol Johnston, and Hassan Ghasemzadeh. 2022. Forewarning Postprandial Hyperglycemia with Interpretations using Machine Learning. *2022 IEEE-EMBS International Conference on Wearable and Implantable Body Sensor Networks (BSN)* (2022), 1–4.

[7] American Heart Association. 2015. *All About Heart Rate (Pulse).* https://www.heart.org/en/health-topics/high-blood-pressure/the-facts-about-high-blood-pressure/all-about-heart-rate-pulse

[8] Ayca Aygun, H. Ghasemzadeh, and R. Jafari. 2020. Robust Interbeat Interval and Heart Rate Variability Estimation Method From Various Morphological Features Using Wearable Sensors. *IEEE Journal of Biomedical and Health Informatics* 24 (2020), 2238–2250.

[9] Ayca Aygun and R. Jafari. 2019. Robust Heart Rate Variability and Interbeat Interval Detection Algorithm in the Presence of Motion Artifacts. *2019 IEEE EMBS International Conference on Biomedical & Health Informatics (BHI)* (2019), 1–5.

[10] M. Bsoul, H. Minn, and L. Tamil. 2011. Apnea MedAssist: Real-time Sleep Apnea Monitor Using Single-Lead ECG. *IEEE Transactions on Information Technology in Biomedicine* 15 (2011), 416–427.

[11] K. Chang and Shing-Hong Liu. 2011. Gaussian Noise Filtering from ECG by Wiener Filter and Ensemble Empirical Mode Decomposition. *Journal of Signal Processing Systems* 64 (2011), 249–264.

[12] Jane Chertoff. 2020. *Why Do Athletes Have a Lower Resting Heart Rate?* https://www.healthline.com/health/athlete-heart-rate

[13] M. Chessa, G. Butera, G. Lanza, E. Bossone, A. Delogu, G. De Rosa, G. Marietti, L. Rosti, and M. Carminati. 2002. Role of Heart Rate Variability in the Early Diagnosis of Diabetic Autonomic Neuropathy in Children. *Herz* 27 (2002), 785–790.

[14] Ramin Fallahzadeh, Mahdi Pedram, and Hassan Ghasemzadeh. 2016. SmartSock: A wearable platform for context-aware assessment of ankle edema. In *2016 38th Annual International Conference of the IEEE Engineering in Medicine and Biology Society (EMBC)*. IEEE, 6302–6306.

[15] Centre for Disease Control and Prevention (CDC). 2020. *Heart Disease Facts.* https://www.cdc.gov/heartdisease/facts.htm

[16] Rahel Gilgen-Ammann, Theresa Schweizer, and T. Wyss. 2019. RR interval signal quality of a heart rate monitor and an ECG Holter at rest and during exercise. *European Journal of Applied Physiology* 119 (2019), 1525–1532.

[17] A. Goldberger, L. Amaral, L. Glass, Jeffrey M. Hausdorff, P. Ivanov, R. Mark, J. Mietus, G. Moody, C. Peng, and H. Stanley. 2000. PhysioBank, PhysioToolkit, and PhysioNet: components of a new research resource for complex physiologic signals. *Circulation* 101 23 (2000), E215–20.

[18] J. Harju, A. Tarniceriu, Jakub Parák, A. Vehkaoja, A. Yli-Hankala, and I. Korhonen. 2018. Monitoring of heart rate and inter-beat intervals with wrist plethysmography in patients with atrial fibrillation. *Physiological measurement* 39 6 (2018), 065007.

[19] M. Hasan, S. Rahman, Asiful Arefeen, T. Ahmed, Mohtasim Nakib, C. Shahnaz, and Arik Subhana. 2019. Portable Real Time ECG Monitor and Disease Diagnostics. *2019 IEEE International Conference on Biomedical Engineering, Computer and Information Technology for Health (BECITHCON)* (2019), 15–19.

[20] Niloofar Hezarjaribi, Sepideh Mazrouee, and Hassan Ghasemzadeh. 2017. Speech2Health: a mobile framework for monitoring dietary composition from spoken data. *IEEE journal of biomedical and health informatics* 22, 1 (2017), 252–264.

[21] Ryan Holder, Ramesh Kumar Sah, Michael Cleveland, and Hassan Ghasemzadeh. 2022. Comparing the predictability of sensor modalities to detect stress from wearable sensor data. In *2022 IEEE 19th Annual Consumer Communications & Networking Conference (CCNC)*. IEEE, 557–562.

[22] Sheng Hu, H. Wei, Y. Chen, and J. Tan. 2012. A Real-Time Cardiac Arrhythmia Classification System with Wearable Sensor Networks. *Sensors (Basel, Switzerland)* 12 (2012), 12844 – 12869.

[23] Shweta Jain, Anil Kumar, and Varun Bajaj. 2017. Real-time detection of electrocardiograph peaks: A genetic algorithm based approach. *2017 4th International Conference on Signal Processing and Integrated Networks (SPIN)* (2017), 262–266.
[24] S. Jégou, M. Drozdzal, David Vázquez, A. Romero, and Yoshua Bengio. 2017. The One Hundred Layers Tiramisu: Fully Convolutional DenseNets for Semantic Segmentation. *2017 IEEE Conference on Computer Vision and Pattern Recognition Workshops (CVPRW)* (2017), 1175–1183.
[25] Eric Jones, Travis Oliphant, Pearu Peterson, et al. 2001–. SciPy: Open source scientific tools for Python. http://www.scipy.org/
[26] A. Karagiannis and P. Constantinou. 2010. On the Empirical Mode Decomposition Performance in White Gaussian Noise Biomedical Signals.
[27] R. Kher. 2019. Signal Processing Techniques for Removing Noise from ECG Signals.
[28] M. Kirst, Bastian Glauner, and J. Ottenbacher. 2011. Using DWT for ECG motion artifact reduction with noise-correlating signals. *2011 Annual International Conference of the IEEE Engineering in Medicine and Biology Society* (2011), 4804–4807.
[29] Pramendra Kumar and Vijay Kumar Sharma. 2020. Detection and classification of ECG noises using decomposition on mixed codebook for quality analysis. *Healthcare Technology Letters* 7 (2020), 18 – 24.
[30] Juho Laitala, Mingzhe Jiang, Elise Syrjälä, Emad Kasaeyan Naeini, Antti Airola, A. Rahmani, N. Dutt, and P. Liljeberg. 2020. Robust ECG R-peak detection using LSTM. *Proceedings of the 35th Annual ACM Symposium on Applied Computing* (2020).
[31] Sunghoon Ivan Lee, Hassan Ghasemzadeh, Bobak Mortazavi, Mars Lan, Nabil Alshurafa, Michael Ong, and Majid Sarrafzadeh. 2013. Remote patient monitoring: what impact can data analytics have on cost?. In *Proceedings of the 4th Conference on Wireless Health*. 1–8.
[32] Yuchao Ma, Zhila Esna Ashari, Mahdi Pedram, Navid Amini, Daniel Tarquinio, Kouros Nouri-Mahdavi, Mohammad Pourhomayoun, Robert D Catena, and Hassan Ghasemzadeh. 2019. CyclePro: A robust framework for domain-agnostic gait cycle detection. *IEEE Sensors Journal* 19, 10 (2019), 3751–3762.
[33] C. McAloon, Luke M Boylan, T. Hamborg, N. Stallard, F. Osman, P. Lim, and S. Hayat. 2016. The changing face of cardiovascular disease 2000-2012: An analysis of the world health organisation global health estimates data. *International journal of cardiology* 224 (2016), 256–264.
[34] Seyed Iman Mirzadeh, Asiful Arefeen, Jessica Ardo, Ramin Fallahzadeh, Bryan Minor, Jung-Ah Lee, Janett A Hildebrand, Diane Cook, Hassan Ghasemzadeh, and Lorraine S Evangelista. 2022. Use of machine learning to predict medication adherence in individuals at risk for atherosclerotic cardiovascular disease. *Smart Health* 26 (2022), 100328.
[35] G. Moody and R. Mark. 2001. The impact of the MIT-BIH Arrhythmia Database. *IEEE Engineering in Medicine and Biology Magazine* 20 (2001), 45–50.
[36] G. Moody, We Muldrow, and R. Mark. 1992. The MIT-BIH Noise Stress Test Database.
[37] Vu Thi Hong Nhan, N. Park, Y. K. Lee, Y. Lee, J. Lee, and K. Ryu. 2010. Online discovery of Heart Rate Variability patterns in mobile healthcare services. *J. Syst. Softw.* 83 (2010), 1930–1940.
[38] J. Pan and W. Tompkins. 1985. A Real-Time QRS Detection Algorithm. *IEEE Transactions on Biomedical Engineering* BME-32 (1985), 230–236.
[39] V. Pandey and V. K. Giri. 2016. High frequency noise removal from ECG using moving average filters. *2016 International Conference on Emerging Trends in Electrical Electronics & Sustainable Energy Systems (ICETEESES)* (2016), 191–195.
[40] A. Pulavskyi, S. Krivenko, and L. S. Kryvenko. 2020. Evaluation of the Effectiveness of Post-filtration Smoothing using Lossless Compression for Heart Rate Variability Obtained from a Very Noisy ECG. *2020 9th Mediterranean Conference on Embedded Computing (MECO)* (2020), 1–5.
[41] Alif Bin Abdul Qayyum, Tanveerul Islam, and M. Haque. 2019. ECG Heartbeat Classification: A Comparative Performance Analysis between One and Two Dimensional Convolutional Neural Network. *2019 IEEE International Conference on Biomedical Engineering, Computer and Information Technology for Health (BECITHCON)* (2019), 93–96.
[42] Lishen Qiu, Wenqiang Cai, Jie Yu, J. Zhong, Yan Wang, Wanyue Li, Y. Chen, and L. Wang. 2020. A two-stage ECG signal denoising method based on deep convolutional network. *bioRxiv* (2020).
[43] Hrishi Rakshit and M. A. Ullah. 2016. A New Efficient Approach for Designing FIR Low-pass Filter and Its Application on ECG Signal for Removal of AWGN Noise.
[44] Shalini A. Rankawat and R. Dubey. 2017. Robust heart rate estimation from multimodal physiological signals using beat signal quality index based majority voting fusion method. *Biomed. Signal Process. Control.* 33 (2017), 201–212.
[45] N. Reljin, J. Lázaro, Md Billal Hossain, Yeon Sik Noh, C. Cho, and K. Chon. 2020. Using the Redundant Convolutional Encoder–Decoder to Denoise QRS Complexes in ECG Signals Recorded with an Armband Wearable Device. *Sensors (Basel, Switzerland)* 20 (2020).
[46] S. Rezk, C. Join, and S. E. Asmi. 2012. Inter-beat (R-R) intervals analysis using a new time delay estimation technique. *2012 Proceedings of the 20th European Signal Processing Conference (EUSIPCO)* (2012), 929–933.
[47] Seyed Ali Rokni and Hassan Ghasemzadeh. 2016. Plug-n-learn: automatic learning of computational algorithms in human-centered internet-of-things applications. In *Proceedings of the 53rd Annual Design Automation Conference*. 1–6.
[48] O. Ronneberger, P. Fischer, and T. Brox. 2015. U-Net: Convolutional Networks for Biomedical Image Segmentation. *ArXiv* abs/1505.04597 (2015).

[49] Ramyar Saeedi, Brian Schimert, and Hassan Ghasemzadeh. 2014. Cost-sensitive feature selection for on-body sensor localization. In *Proceedings of the 2014 ACM International Joint Conference on Pervasive and Ubiquitous Computing: Adjunct Publication*. 833–842.
[50] Ramesh Kumar Sah, Michael John Cleveland, Assal Habibi, and Hassan Ghasemzadeh. 2022. Stressalyzer: Convolutional Neural Network Framework for Personalized Stress Classification. In *2022 44th Annual International Conference of the IEEE Engineering in Medicine & Biology Society (EMBC)*. IEEE, 4658–4663.
[51] Vinu Sundararaj. 2016. An Efficient Threshold Prediction Scheme for Wavelet Based ECG Signal Noise Reduction Using Variable Step Size Firefly Algorithm. *International Journal of Intelligent Engineering and Systems* 9 (2016), 117–126.
[52] A. Taddei, G. Distante, M. Emdin, P. Pisani, G. Moody, C. Zeelenberg, and C. Marchesi. 1992. The European ST-T database: standard for evaluating systems for the analysis of ST-T changes in ambulatory electrocardiography. *European heart journal* 13 9 (1992), 1164–72.
[53] M. Talbi, S. Abid, and A. Cherif. 2015. EMD-BASED ECG DENOISING USING SOURCE SEPARATION. *Journal of Mechanics in Medicine and Biology* 15 (2015), 1550082.
[54] L. Tereshchenko and M. Josephson. 2015. Frequency content and characteristics of ventricular conduction. *Journal of electrocardiology* 48 6 (2015), 933–7.
[55] C. Varon, A. Caicedo, D. Testelmans, B. Buyse, and S. Huffel. 2015. A Novel Algorithm for the Automatic Detection of Sleep Apnea From Single-Lead ECG. *IEEE Transactions on Biomedical Engineering* 62 (2015), 2269–2278.
[56] Sricharan Vijayarangan, Vignesh Ravichandran, Balamurali Murugesan, S. Preejith, J. Joseph, and M. Sivaprakasam. 2020. RPnet: A Deep Learning approach for robust R Peak detection in noisy ECG. *2020 42nd Annual International Conference of the IEEE Engineering in Medicine & Biology Society (EMBC)* (2020), 345–348.
[57] World Health Organization (WHO). 2017. *Cardiovascular diseases (CVDs)*. https://www.who.int/news-room/fact-sheets/detail/cardiovascular-diseases-(cvds)
[58] Zhe Yang, Qihao Zhou, L. Lei, K. Zheng, and Wei Xiang. 2016. An IoT-cloud Based Wearable ECG Monitoring System for Smart Healthcare. *Journal of Medical Systems* 40 (2016), 1–11.
[59] B. Yuen, X. Dong, and Tao Lu. 2020. Detecting Noisy ECG QRS Complexes Using WaveletCNN Autoencoder and ConvLSTM. *IEEE Access* 8 (2020), 143802–143817.
[60] Zhilin Zhang, Zhouyue Pi, and B. Liu. 2015. TROIKA: A General Framework for Heart Rate Monitoring Using Wrist-Type Photoplethysmographic Signals During Intensive Physical Exercise. *IEEE Transactions on Biomedical Engineering* 62 (2015), 522–531.

A ONLINE RESOURCES

The code for this paper can be found at: https://github.com/Arefeen06088/IBI_Tiramisu